Optical and Quantum Electronics **33:** 327–341, 2001.

Optical modelling of photonic crystals and VCSELs using eigenmode expansion and perfectly matched layers

P. BIENSTMAN* AND R. BAETS
*Department of Information Technology/IMEC, Ghent University, Sint-Pietersnieuwstraat 41, Ghent, Belgium (*author for correspondence, E-mail: peter.bienstman@rug.ac.be)*

Abstract. We present a modelling approach for photonic crystal structures and vertical-cavity surface-emitting lasers (VCSELs). This method is based on vectorial eigenmode expansion combined with perfectly matched layer (PML) boundary conditions. Compared to other methods, a relatively small computational effort is required, while at the same time accurate results are obtained, even in the presence of strong scattering and diffraction losses.

Key words: absorbing boundary conditions, eigenmode expansion, photonic crystals, PML, VCSEL

1. Introduction

For the modelling of optical structures, a large variety of methods abound. On one hand, there exist a number of approximate models that are typically quite fast. However, they have a restricted domain of validity. The beam propagation method (BPM) e.g. is mainly limited to structures with small refractive index contrasts or that exhibit dominant paraxial propagation.

On the other hand, there is a large class of models where Maxwell's equations are solved exactly, the only approximation being the finite mesh size or the finite number of terms retained in a series expansion. Most of these models are based on spatially discretising the structure under study. However, most interesting structures require a large number of grid points to model accurately, so that they introduce a large number of unknowns to be solved for. Needless to say that these models typically tend to be quite slow, making them less suitable for use in a design process requiring a large number of iterations. Models in this class include e.g. the finite-difference time-domain method, other methods based on finite elements or finite differences, or hybrid models like the method of lines (MoL). For an excellent overview of these techniques, we refer to Scarmozzino *et al.* (2000) and the references therein.

In order to reduce the computational effort of these exact models, we can use to our advantage the fact that most structures can be represented by a refractive index profile that is piecewise constant. This fact is exploited in eigenmode expansion methods (Sztefka and Nolting 1993) (also called mode-matching methods), where the structures are sliced up in a number of layers in which the index profile does not change in the propagation direction z (Fig. 1). In each of these layers, the field is expanded onto the set of eigenmodes of that particular layer. Since these can be calculated analytically, no spatial discretisation is required, giving rise to only a small number of unknowns and a therefore a fast model.

However, in order to get a discrete set of radiation modes, these methods require the structure to be enclosed in a metal volume. This has been the main problem plaguing eigenmode expansion techniques in the past, since the radiated fields are completely reflected back into the structure.

To alleviate this, it was recently proposed to coat the metal volume with a perfectly matched layer (PML) (Derudder 1998; Bienstman *et al.* 2001). Contrary to traditional absorbers, PMLs give reflectionless absorption of the incident field, regardless of wavelength, polarisation or incidence angle.

In this paper, we give an outline of our modelling approach, based on eigenmode expansion and PMLs, and illustrate it with a number of examples on periodically etched waveguides and oxide-confined vertical-cavity surface-emitting lasers (VCSELs).

2. Description of the model

The modelling of an optical structure using this method proceeds in a number of steps:

- In each layer, find the local eigenmodes that will be used to expand the field.

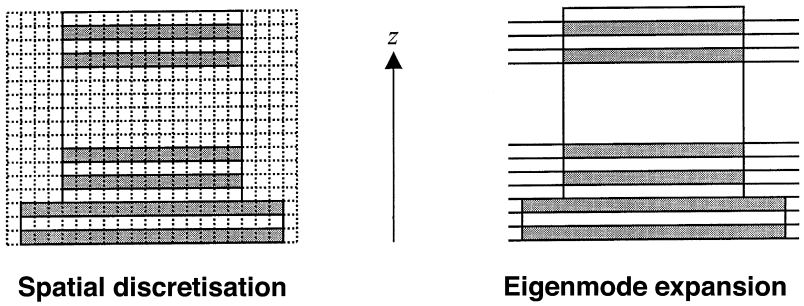

Fig. 1. Spatial discretisation vs. eigenmode expansion.

- For each interface between two layers, calculate the reflection and transmission matrices that describe mode conversion and scattering at that interface.
- For a given stack of layers, calculate the reflection and transmission matrices of the entire stack.

Once we have this information, we can additionally also

- Look for resonator (laser) modes of a cavity defined by two stacks.
- Calculate the field profile inside a stack for any given excitation.
- Calculate the band diagram of the Bloch modes appearing for an infinite repetition of given stack.

These steps will now be described in more detail.

2.1. EIGENMODES IN EACH LAYER

In each layer, any arbitrary field can be written as a linear combination of the forward ('+') and the backward ('−') propagating eigenmodes of that particular layer:

$$\begin{aligned}\mathbf{E}(\mathbf{r}_t, z) &= \sum_k \left\{A_k^+ \mathbf{E}_k(\mathbf{r}_t)\exp(-\mathrm{j}\beta_k z) + A_k^- \mathbf{E}_k(\mathbf{r}_t)\exp(\mathrm{j}\beta_k z)\right\}\\ \mathbf{H}(\mathbf{r}_t, z) &= \sum_k \left\{A_k^+ \mathbf{H}_k(\mathbf{r}_t)\exp(-\mathrm{j}\beta_k z) - A_k^- \mathbf{H}_k(\mathbf{r}_t)\exp(\mathrm{j}\beta_k z)\right\}\end{aligned} \tag{1}$$

Here $\mathbf{r}_t$ is the transverse coordinate, the direction of propagation is z and β represents the propagation constants of the eigenmodes. Theoretically, these sums run from $k = 1$ to infinity, but we terminate the series at a given index N.

Any 3D field distribution in that particular layer can therefore be represented very compactly by a vector $\mathbf{A}$ containing the expansion coefficients, without resorting to spatial discretisation.

To determine the propagation constants of the eigenmodes, one typically has to solve a transcendental dispersion relation.

2.2. PML BOUNDARY CONDITIONS

We include the presence of PML boundary conditions when we formulate the transcendental dispersion relation satisfied by the propagation constants of the eigenmodes. It was shown in Chew *et al.* (1997) that a PML-layer could be described as an isotropic, lossless layer, but with a complex thickness. The imaginary part of this thickness provides for reflectionless absorption of the incident field, regardless of its wavelength, incidence angle or polarisation.

The advantage of such a formulation is that expressions derived in situations without PML can be simply extended to include PML by allowing the outer regions of the computational domain to have a complex thickness.

Fig. 2 shows the influence of PML on the distribution in the complex n_{eff}-plane of the propagation constants of a waveguide with a circular geometry. The core has a radius $r = 0.5\,\mu\text{m}$ and consists of AlAs with refractive index $n_1 = 2.9$. The cladding is AlOx ($n_2 = 1.55$) and the metal cylinder has a radius $\tilde{R} = 1.0 - 0.1j\,\mu\text{m}$. The wavelength is 1 μm, and the modes shown have Bessel order 1.

It can be seen from Fig. 2 that the influence of PML on the guided modes is negligible. They are still located on their original place on the real n_{eff}-axis. The radiation modes on the other hand are no longer distributed along the coordinate axes, but are located on four branches in the complex plane.

For more details on the mode structure and profiles of these eigenmodes in the presence of PML, including on efficient numerical techniques to locate them, we refer to (Derudder *et al.* 1998; Bienstman *et al.* 2001).

2.3. INTERFACES BETWEEN TWO LAYERS

The derivation of the scattering matrix of an interface proceeds by the well-known mode-matching technique (see e.g. Zaki *et al.* 1988). Suppose an interface between two waveguides I and II is placed at $z = 0$ and that a single

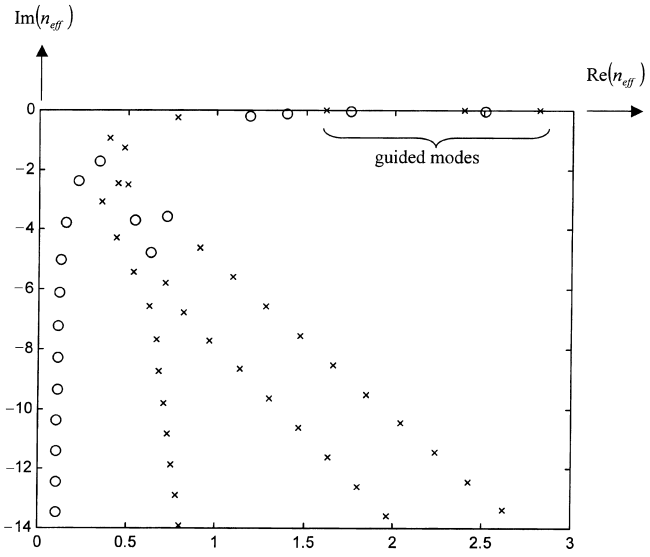

Fig. 2. Influence of PML on the distribution of propagation constants in the n_{eff}-plane (circles: EH modes, crosses: HE modes).

mode p of waveguide I is incident upon this interface (Fig. 3). In both waveguides we retain the same number N modes of modes. Expressing the continuity of the tangential field components leads to:

$$\begin{aligned}
&\mathbf{E}^{\mathrm{I}}_{p,\tan}(\mathbf{r}_t) + \sum_j R_j \mathbf{E}^{\mathrm{I}}_{j,\tan}(\mathbf{r}_t) = \sum_j T_j \mathbf{E}^{\mathrm{II}}_{j,\tan}(\mathbf{r}_t) \\
&\mathbf{H}^{\mathrm{I}}_{p,\tan}(\mathbf{r}_t) - \sum_j R_j \mathbf{H}^{\mathrm{I}}_{j,\tan}(\mathbf{r}_t) = \sum_j T_j \mathbf{H}^{\mathrm{II}}_{j,\tan}(\mathbf{r}_t)
\end{aligned} \tag{2}$$

For every index i from 1 to N, we now take the right vectorial product of the first equation with $\mathbf{H}^{\mathrm{I}}_{i,\tan}$ and the left vectorial product of the second equation with $\mathbf{E}^{\mathrm{I}}_{i,\tan}$. Integrating over the transverse cross section and invoking orthogonality finally leads to a system from which the unknown reflection and transmission coefficients can be determined:

$$\begin{aligned}
&\sum_j \left[\left\langle \mathbf{E}^{\mathrm{I}}_i \cdot \mathbf{H}^{\mathrm{II}}_j \right\rangle + \left\langle \mathbf{E}^{\mathrm{II}}_j \cdot \mathbf{H}^{\mathrm{I}}_i \right\rangle \right] T_j = 2\delta_{ip} \left\langle \mathbf{E}^{\mathrm{I}}_p \cdot \mathbf{H}^{\mathrm{I}}_p \right\rangle \\
&R_i = \frac{1}{2\left\langle \mathbf{E}^{\mathrm{I}}_i \cdot \mathbf{H}^{\mathrm{I}}_i \right\rangle} \sum_j \left[\left\langle \mathbf{E}^{\mathrm{II}}_j \cdot \mathbf{H}^{\mathrm{I}}_i \right\rangle - \left\langle \mathbf{E}^{\mathrm{I}}_i \cdot \mathbf{H}^{\mathrm{II}}_j \right\rangle \right] T_j
\end{aligned} \tag{3}$$

The scalar product is defined as an overlap integral over the cross-section:

$$\langle \mathbf{E} \cdot \mathbf{H} \rangle = \iint_S \mathbf{E} \times \mathbf{H} \cdot \mathbf{u}_z \, \mathrm{d}S \tag{4}$$

This procedure is repeated for any incident mode p, until finally we arrive at reflection and transmission matrices:

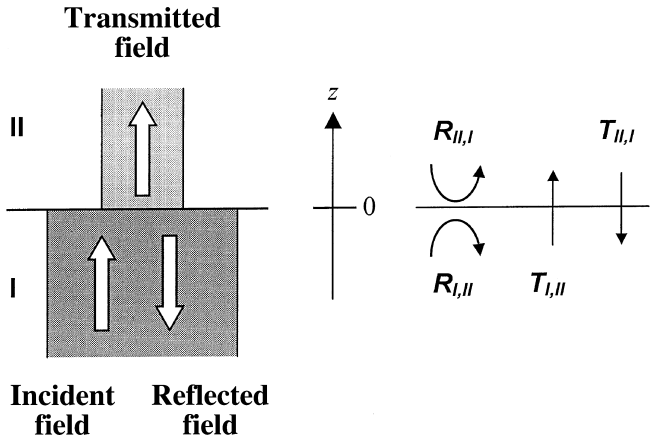

Fig. 3. Interface between two waveguides.

$$\begin{aligned}\bar{A}_{\text{refl}} &= \bar{\bar{R}}_{\text{I,II}} \cdot \bar{A}_{\text{inc}} \\ \bar{A}_{\text{trans}} &= \bar{\bar{T}}_{\text{I,II}} \cdot \bar{A}_{\text{inc}}\end{aligned} \tag{5}$$

Similar expressions are derived for the case with incidence from medium II. Together, these four matrices are submatrices of the scattering matrix, which completely characterises the interface.

2.4. STACK OF LAYERS

A stack consists of a sequence of layers and each layer in turn consists of an interface, whose behaviour is characterised by the reflection and transmission matrices from (5), and a given length of waveguide, where the propagation of the field is given by (1).

For the determination of the R and T-matrices of the entire stack, one can either use the transfer matrix formalism or the scattering matrix formalism (Li 1996). The transfer matrix formalism relates the forward and the backward waves at the beginning of a substack to the forward and backward waves at the end of the substack. Although this method is conceptually simple, it is numerically unstable for evanescent modes, since the expressions combine both increasing and decreasing exponentials $\exp(\pm \mathrm{j}\beta z)$.

It is therefore better to use a scattering matrix formalism, which relates the incident fields (i.e. forward field at the beginning and backward field at the end) to the outgoing fields (i.e. backward field at the beginning and forward field at the end).

The procedure recursively determines the reflection and transmission (i.e. scattering) matrices of the first $p+1$ layers, given these matrices for the first p layers:

First, the following matrices are calculated (Li 1996):

$$\begin{aligned}\bar{\bar{t}}_{p+1,p} &= \bar{\bar{T}}_{p+1,p} \cdot \operatorname{diag}\left(\exp\left(-\mathrm{j}\beta_{p+1} d_{p+1}\right)\right) \\ \bar{\bar{r}}_{p,p+1} &= \bar{\bar{R}}_{p,p+1} \\ \bar{\bar{r}}_{p+1,p} &= \operatorname{diag}\left(\exp\left(-\mathrm{j}\beta_{p+1} d_{p+1}\right)\right) \cdot \bar{\bar{R}}_{p+1,p} \cdot \operatorname{diag}\left(\exp\left(-\mathrm{j}\beta_{p+1} d_{p+1}\right)\right) \\ \bar{\bar{t}}_{p,p+1} &= \operatorname{diag}\left(\exp\left(-\mathrm{j}\beta_{p+1} d_{p+1}\right)\right) \cdot \bar{\bar{T}}_{p,p+1}\end{aligned} \tag{6}$$

The diagonal matrices express the propagation of the modes in layer $p+1$ over the distance given by its thickness d_{p+1}. Note that only exponentials with the same sign occur in the formulas. This accounts for its numerical stability.

Finally, the matrices describing the first $p+1$ layers are given by:

$$\begin{aligned}
\bar{\bar{T}}_{p+1,1} &= \bar{\bar{T}}_{p,1} \cdot \left[\bar{\bar{1}} - \bar{\bar{r}}_{p,p+1} \cdot \bar{\bar{R}}_{p,1}\right]^{-1} \cdot \bar{\bar{t}}_{p+1,p} \\
\bar{\bar{R}}_{1,p+1} &= \bar{\bar{T}}_{p,1} \cdot \left[\bar{\bar{1}} - \bar{\bar{r}}_{p,p+1} \cdot \bar{\bar{R}}_{p,1}\right]^{-1} \cdot \bar{\bar{r}}_{p,p+1} \cdot \bar{\bar{T}}_{1,p} + \bar{\bar{R}}_{1,p} \\
\bar{\bar{R}}_{p+1,1} &= \bar{\bar{t}}_{p,p+1} \cdot \left[\bar{\bar{1}} - \bar{\bar{R}}_{p,1} \cdot \bar{\bar{r}}_{p,p+1}\right]^{-1} \cdot \bar{\bar{R}}_{p,1} \cdot \bar{\bar{t}}_{p+1,p} + \bar{\bar{r}}_{p+1,p} \\
\bar{\bar{T}}_{1,p+1} &= \bar{\bar{t}}_{p,p+1} \cdot \left[\bar{\bar{1}} - \bar{\bar{R}}_{p,1} \cdot \bar{\bar{r}}_{p,p+1}\right]^{-1} \cdot \bar{\bar{T}}_{1,p}
\end{aligned} \tag{7}$$

Of course, the same method can be applied to concatenate substacks. The R and T matrices then represent the properties of a substack instead of those of a single interface and the thicknesses d should be chosen zero.

2.5. PERIODIC STRUCTURES

An important advantage of eigenmode expansion techniques is that they allow for an efficient algorithm if some substacks exhibit periodicity. This is especially useful when studying e.g. DBR mirrors or photonic crystals.

Suppose we have a basic stack S that is repeated N times. A straightforward way of calculating the properties of the entire stack would be to first calculate the R and T matrices of S and then concatenate N copies of the basic period:

$$S_N = S \otimes S \otimes \cdots \otimes S \quad (N \text{ times}) \tag{8}$$

The operator $\otimes$ stands for concatenation of two substacks using the scattering matrix formalism.

A faster way is to make use of the following recurrence[1] relations

$$\begin{aligned}
S_{2i} &= S_i \otimes S_i \\
S_{2i+1} &= S_{2i} \otimes S
\end{aligned} \tag{9}$$

In this way, the calculation time is logarithmic in the number of periods instead of linear. The time savings can be substantial, especially in the case of a large number of periods. (The case of an infinite number of periods is treated further in the text.)

[1] For computer implementation, it is of course advantageous to reformulate this recursive relation as an iterative expression.

2.6. LASER CAVITIES

We can now proceed to calculate the threshold material gain and lasing wavelength of a resonator, e.g. a laser cavity. We first divide the resonator at an arbitrary plane in a top and a bottom stack (Fig. 4). Then, we calculate the reflection matrix R_{top} of the top part as seen from the bottom and also the reflection matrix R_{bot} of the bottom part as seen from the top. A laser mode A_{lasing} satisfies the condition that its roundtrip gain equals unity:

$$\bar{\bar{R}}_{\text{top}} \cdot \bar{\bar{R}}_{\text{bot}} \cdot \bar{A}_{\text{lasing}} = \bar{A}_{\text{lasing}} \tag{10}$$

This means that we have to sweep wavelength and gain in the resonator in order to get an eigenvector of the matrix $R_{\text{top}} \cdot R_{\text{bot}}$ with an eigenvalue of one.

In Demeulenaere *et al.* (1999), we showed that for reasons of numerical stability, it can be advantageous to reformulate this problem in terms of a singular value decomposition (SVD) of the matrix

$$\bar{\bar{1}} - \bar{\bar{R}}_{\text{top}} \cdot \bar{\bar{R}}_{\text{bot}} \tag{11}$$

A singular value equal to zero of this new matrix corresponds to an eigenvalue equal to one of the original matrix.

In Demeulenaere *et al.* (1999), it was also shown that the two-dimensional search for a laser mode in the (wavelength, gain) – domain can be successfully done by first doing a wavelength sweep to achieve phase resonance and subsequently a gain sweep to obtain amplitude resonance.

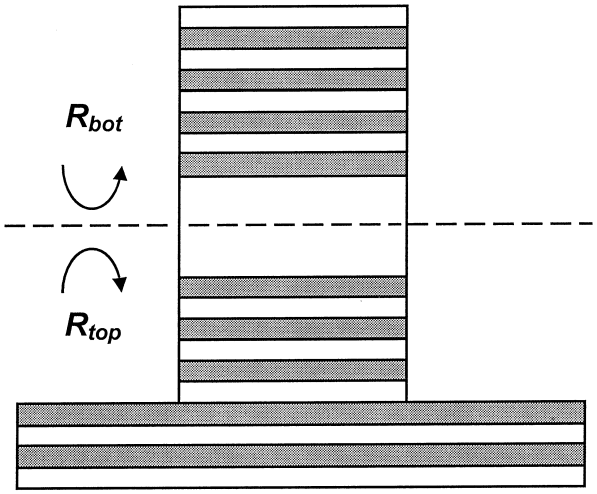

Fig. 4. A laser cavity.

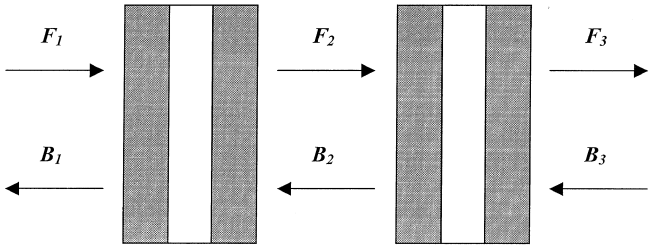

Fig. 5. Calculating field profiles inside a stack.

2.7. FIELD PROFILES

Suppose we excite a stack with an incident field F_1 coming from the left. This will give rise to a reflected field $B_1 = R_{\text{stack,total}} \cdot F_1$ (Fig. 5). If we want to calculate the forward and the backward fields at an interior position 2 inside the stack, we can proceed in two ways.

A first way is to start from

$$\begin{aligned} \bar{B}_1 &= \bar{\bar{R}}_{12} \cdot \bar{F}_1 + \bar{\bar{T}}_{21} \cdot \bar{B}_2 \\ \bar{F}_2 &= \bar{\bar{R}}_{21} \cdot \bar{B}_2 + \bar{\bar{T}}_{12} \cdot \bar{F}_1 \end{aligned} \tag{12}$$

which gives for the unknown fields

$$\begin{aligned} \bar{F}_2 &= \left[\bar{\bar{T}}_{12} - \bar{\bar{R}}_{21} \cdot \bar{\bar{T}}_{21}^{-1} \cdot \bar{\bar{R}}_{12}\right] \bar{F}_1 + \bar{\bar{R}}_{21} \cdot \bar{\bar{T}}_{21}^{-1} \cdot B_1 \\ \bar{B}_2 &= -\bar{\bar{T}}_{21}^{-1} \cdot \bar{\bar{R}}_{12} \cdot \bar{F}_1 + \bar{\bar{T}}_{21}^{-1} \cdot \bar{B}_1 \end{aligned} \tag{13}$$

For a position deep inside the stack however, T_{21} can become numerically close to singular. This is due to higher order modes, which will be totally internally reflected and therefore have zero transmission. This introduces a number close to zero on the diagonal of an otherwise diagonally dominant matrix.

An alternative therefore is to also consider the right part of the stack, between positions 2 and 3.

$$\begin{aligned} \bar{F}_2 &= \bar{\bar{R}}_{21} \cdot \bar{B}_2 + \bar{\bar{T}}_{12} \cdot \bar{F}_1 \\ \bar{B}_2 &= \bar{\bar{R}}_{23} \cdot \bar{F}_2 + \bar{\bar{T}}_{32} \cdot \bar{B}_3 \end{aligned} \tag{14}$$

In the absence of an incident field B_3 in medium 3, we can therefore write

$$\begin{aligned} \bar{F}_2 &= \left[\bar{\bar{1}} - \bar{\bar{R}}_{21} \cdot \bar{\bar{R}}_{23}\right]^{-1} \cdot \bar{\bar{T}}_{12} \cdot \bar{F}_1 \\ \bar{B}_2 &= \bar{\bar{R}}_{23} \cdot \bar{F}_2 \end{aligned} \tag{15}$$

In this case, we avoid inverting T_{21}. The matrix that we now invert only becomes singular in case the entire stack contains a lasing resonance. Note that this is rarely a problem, not even when plotting field profiles of a lasing mode. In this case we start from the field profiles in the middle of the stack and propagate them through either the top or the bottom mirror, which by themselves do not exhibit lasing resonances.

2.8. BLOCH MODES

With the knowledge of the R and T matrices of a given stack, it is also straightforward to determine the Bloch modes that arise when infinitely repeating this stack.

Starting from (12), we impose periodic boundary conditions in the z-direction:

$$\begin{aligned} \bar{F}_2 &= \alpha \bar{\bar{F}}_1 \\ \bar{B}_2 &= \alpha \bar{\bar{B}}_1 \end{aligned} \tag{16}$$

Combining (12) and (16) leads to an eigenvalue equation for the Bloch modes:

$$\begin{bmatrix} \bar{\bar{T}}_{12} - \bar{\bar{R}}_{21} \cdot \bar{\bar{T}}_{21}^{-1} \cdot \bar{\bar{R}}_{12} & \bar{\bar{R}}_{21} \cdot \bar{\bar{T}}_{21}^{-1} \\ -\bar{\bar{T}}_{21}^{-1} \cdot \bar{\bar{R}}_{12} & \bar{\bar{T}}_{21}^{-1} \end{bmatrix} \cdot \begin{bmatrix} \bar{F}_1 \\ \bar{B}_1 \end{bmatrix} = \alpha \begin{bmatrix} \bar{F}_1 \\ \bar{B}_1 \end{bmatrix} \tag{17}$$

The eigenvectors give the field profiles of the Bloch modes, while their propagation constants follow from

$$\alpha_i = \exp(-\mathrm{j}\beta_i d) \tag{18}$$

with d the thickness of the basic period.

If we use for the transverse boundary conditions also periodic ones, or suitable combinations of classical electric and magnetic walls, we can calculate the band structure of photonic crystals that extend infinitely in both the longitudinal and transverse direction. When using a PML transverse boundary condition however, we are now also able to calculate e.g. the radiation losses in Bloch modes of structures that are only periodic in the z-direction. The presence of the PML will absorb the radiation losses instead of reflecting them, giving rise to an imaginary component in the propagation constants (without PML they would have been real for lossless materials). The determination of radiation losses is something that is not possible using other methods.

3. CAMFR

From the previous discussion, it is clear that the algorithms outlined above can be applied equally well to any geometry, be it a cartesian geometry or a circular symmetric one. We can use this to our advantage when implementing a CAD tool, since most of the algorithms do not need to be aware of the specific geometry they are operating on. They can therefore be reused for any geometry.

We have developed an abstract framework based on these principles called CAMFR, short for CAvity Modelling FRamework. We are currently able to deal with arbitrary 2D cartesian structures (for the modelling of photonic crystal structures) and circular symmetric devices with a single radial index step (for the modelling of VCSELs).

We will now illustrate the model with two examples. The first one deals with a periodically etched waveguide grating, while the second treats the position dependent effects of thin oxide apertures in VCSELs.

4. Example: waveguide grating

Consider the following structure, originating from the European COST 268 action (Fig. 6). It is a Si_3N_4 waveguide on a SiO_2 substrate, with a 20 period grating etched into it. For the details on the material parameters, we refer to Čtyroký.

For a shallow etch of 125 μm, Fig. 7 shows the calculated reflection R and transmission T of the fundamental mode of this waveguide, as well as its loss $L = 1 - R - T$. The thickness of the substrate was chosen to be $7.5 - 0.15j\,\mu m$, with the imaginary part providing PML absorption. Similarly, the thickness of the air cladding was chosen to be $5 - 0.15j\,\mu m$.

The formation of a stop band around 1.5 μm is clearly visible.

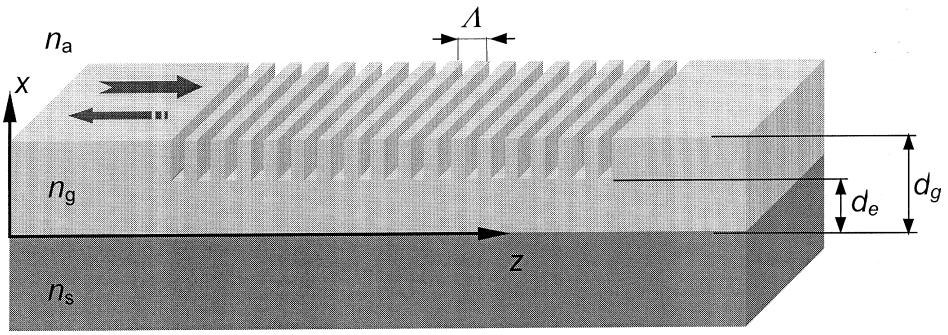

Fig. 6. Waveguide with etched grating.

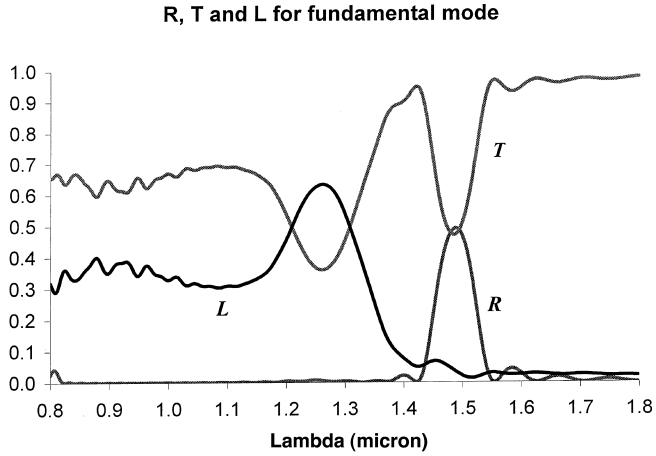

Fig. 7. Reflectivity, transmittivity and radiation losses for fundamental mode.

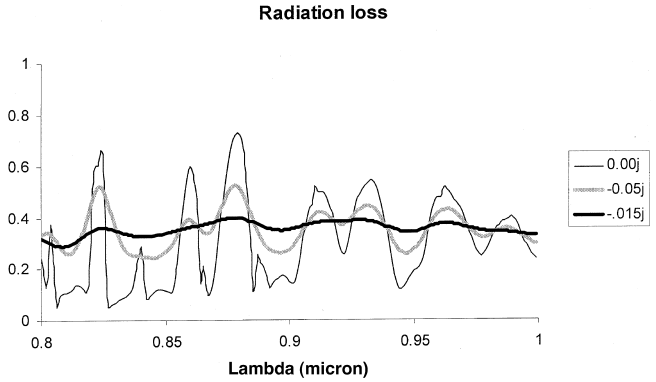

Fig. 8. Radiation losses for varying imaginary thickness (in μm) of the PML.

To illustrate the effect of PML, we now plot in Fig. 8 the radiation losses for different values of the imaginary part of the cladding layer thickness. For $d_{\text{imag}} = 0$, i.e. the case without PML, it is obvious that the parasitic reflections at the metal walls give rise to very large oscillations, ranging almost between zero and unity radiation loss. The inclusion of PML significantly damps these oscillations, and allows for a correct calculation of the radiation losses.

The number of modes used in the calculation of Fig. 8 equals $120/\lambda$. To investigate the series truncation error, we plot in Fig. 9 the radiation loss at 0.9 μm as a function of the number of modes retained in the series expansion, both without PML and with $d_{\text{imag}} = -0.15$. The two curves exhibit very similar convergence behaviour. However, without PML the loss converges to an erroneous value due to the influence of parasitic reflections. Without resorting to PML, this error can only be reduced by increasing the distance between the metal walls, at the expense of requiring a higher number of

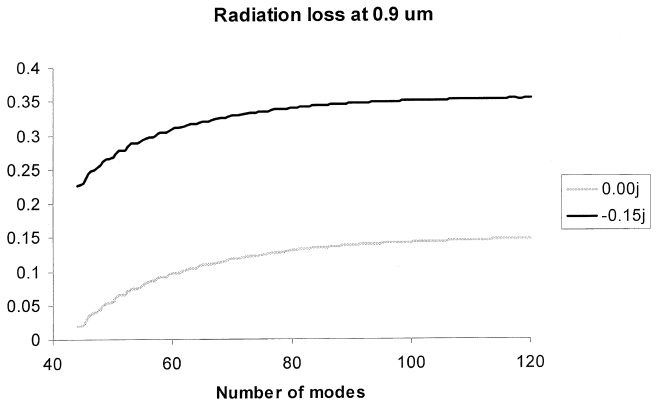

Fig. 9. Convergence properties of radiation loss, both with and without PML.

modes. We can conclude therefore that PML allows for a significantly faster model, because the computational domain can be chosen much smaller with the benefit of a reduced number of modes required.

5. Example: oxide confined VCSEL

We now investigate a GaAs/AlGaAs 980 nm VCSEL structure with circular symmetry (Fig. 10). A thin oxide aperture is placed in five different positions in the cavity, ranging from a node position (1) to an antinode position (5).

For more details on the material and geometry parameters of this device, also a modelling exercise from the COST 268 action, we refer to COST 268 working group.

In Fig. 11, the threshold material gain for a 4 μm radius VCSEL is plotted as a function of the oxide position. The lowest thresholds are observed for an antinode oxide. Indeed, when placed at the field maximum, the waveguiding effect of the oxide is very effective in counteracting diffraction.

If the radius of the VCSEL becomes too small however, diffraction and scattering losses at the aperture will increase, leading to a large increase in

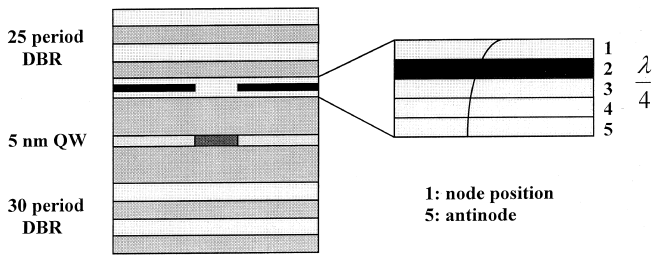

Fig. 10. Oxide confined VCSEL.

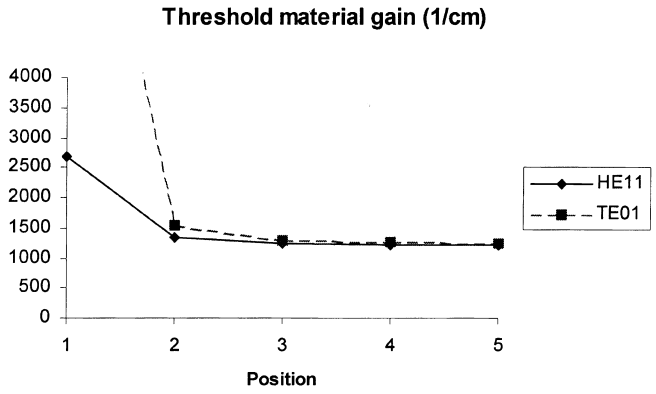

Fig. 11. Threshold material gain for fundamental and first order mode as a function of oxide position.

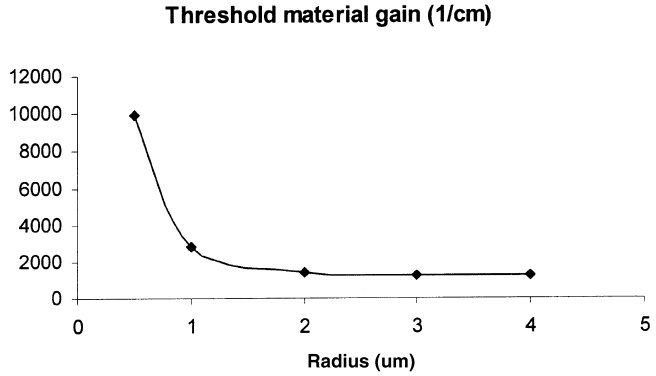

Fig. 12. Threshold material gain as a function of VCSEL radius.

threshold (Demeulenaere *et al.* 1999). This is illustrated in Fig. 12, showing the threshold gain for an antinode oxide as a function of device radius.

6. Conclusion

We presented a modelling approach for photonic crystal structures and VCSELs. Due to the use of eigenmode expansion instead of spatial discretisation, this model is computationally efficient. Thanks to the incorporation of PML boundary conditions, the influence of parasitic reflections can be minimised and radiation losses can be calculated accurately.

Acknowledgements

PB acknowledges support from the Flemish National Fund for Scientific Research (FWO-Vlaanderen). Parts of this work were carried out in the

framework of the Belgian DWTC project IUAP IV-13 and the European COST 268 action.

References

Bienstman, P., H. Derudder, R. Baets, F. Olyslager and D. De Zutter. *IEEE Trans. Microwave Theory Tech.* **49** 349, 2001.

Chew, W.C., J.M. Jin and E. Michielssen. *Microwave Opt. Technol. Lett.* **15** 363, 1997.

Ctyroky, J. COST 268 working group. 2 modelling exercise (http://www.ure.cas.cz/dpt130/cost268/).

COST 268 working group. 1 modelling exercise (http://www.ele.kth.se/COST268/WG1/WGExcercise1.html).

Demeulenaere, B., P. Bienstman, B. Dhoedt and R. Baets. *IEEE J. Quantum Electron.* **35** 358, 1999.

Derudder, H., F. Olyslager and D. De Zutter. *Electronic Lett.* **34** 2138, 1998.

Derudder, H., F. Olyslager, D. De Zutter and S. Van Den Berghe. *IEEE Trans. Antennas Propagat.* (in press).

Li, L. *J. Opt. Soc. Am. A* **13** 1024, 1996.

Scarmozzino, R., A. Gopinath, R. Pregla and S. Helfert. *IEEE J. Selected Topics in Quantum Electron.* **6** 150, 2000.

Sztefka, G. and H.P. Nolting. *IEEE Photon. Technol. Lett.* **5** 554, 1993.

Zaki, K.A., S.W. Chen and C. Chen. *IEEE Trans. Microwave Theory Tech.* **36** 1804, 1988.